PROCEEDINGS, 49th Workshop on Geothermal Reservoir Engineering
Stanford University, Stanford, California, February 12-14, 2024
SGP-TR-227

Near-Wellbore DEM Model of Hydraulic Fracture Initiation for Utah FORGE Site

Wei Fu[1], Branko Damjanac[1], Zorica Radakovic-Guzina[1], Aleta Finnila[2], Robert Podgorney[3], John Mclennan[4]

1 Itasca Consulting Group, Inc., Minneapolis, MN, USA

wei@itascacg.com

2 WSP USA, Inc., Redmond, WA, USA

aleta.finnila@wsp.com

3 Idaho National Laboratory, Idaho Falls, ID, USA

robert.podgorney@inl.gov

4 Department of Chemical Engineering, University of Utah, Salt Lake City, UT, USA

jmclennan@egi.utah.edu

Keywords: Near-Wellbore Tortuosity, Cement Sheath, Perforation, Discrete Fracture Network (DFN), Enhanced Geothermal System (EGS)

ABSTRACT

Three stimulation stages were performed in 2022 near the toe of well 16A(78)-32 at the Utah FORGE site, consisting of two cased-hole sections and one open-hole section. An important aspect of cased-hole completion is to perforate the well casing to establish flow paths between the wellbore and the adjacent reservoir. In the two cased-hole sections, single 20-ft long perforation clusters with six shots per foot at 60° phasing were used, along with bridge plugs for stage isolation. The placement of the perforations, together with the complex stress field resulting from subsurface in-situ stresses and stress concentrations around the wellbore and perforation tunnels, can significantly influence the near-wellbore fracture geometry, which, in turn, directly impacts fluid flow efficiency into and out of the well. Building upon field tests, we have developed numerical models for the Utah FORGE Site to explore the near-wellbore fracture geometry and fluid pressure characteristics. The numerical models use a discrete element modeling (DEM) approach to explicitly represent the well casing, cement sheath, and perforation tunnels. Numerical simulations are performed to investigate fracture initiation from perforation tunnels. The modeling results demonstrate complex fracture behaviors highlighting the competition and merging of fractures and illustrate the important roles of cement strength and discrete fracture network (DFN) in the near-wellbore growth of hydraulic fractures.

1. INTRODUCTION

FORGE, located near Milford, Utah, is a U.S. Department of Energy funded project with the objectives of developing and testing techniques for creating, sustaining, and monitoring Enhanced Geothermal System (EGS) reservoirs (McLennan et al. 2023). In April of2022, three stages of reservoir stimulation by fluid injection were performed at the toe of the injection well 16A(78)-32. Different well completion approaches were utilized, including the open-hole approach at Stage 1 and the case-hole approach at Stages 2 and 3. An important aspect of cased-hole completion is to perforate the well casing to establish flow paths, through which fluids interact with the hot rock formations. Gaining a good understanding of the efficacy of the perforation completion design is essential because the resulting hydraulic fracture characteristics near the wellbore can influence several critical aspects in EGS, such as reservoir connectivity, fluid circulation, proppant transportation, and the efficiency of geothermal energy production.

Modeling the near-wellbore fracture initiation and propagation has been challenging due to complex influencing factors that need to be captured by a model, including the properties of casing-cement sheath-rock structure, phasing and length of perforation tunnels, interference of hydraulic fractures from different perforations, interactions between hydraulic and natural fractures, in-situ stress conditions, etc. It is also necessary for the model to span multiple scales in order to capture different behaviors from fracture initiation along perforation tunnels at a millimeter scale to fracture propagation near the wellbore at a meter scale, which brings significant computational challenges. In this study, numerical models were developed based on the Utah FORGE Site to explore the near-wellbore fracture characteristics. Using a discrete element modeling (DEM) lattice approach, we studied the influence of well perforation, cementation strengths, and discrete fracture network (DFN) on hydraulic fracture initiation and propagation, with well casing, cement sheath, and perforation tunnels explicitly represented in the models.

2. ENGINEERING BACKGROUND

At the Utah FORGE site, injection well 16A(78)-32 has been drilled with an inclination angle of 65° to the vertical, and a three-stage fracturing treatment was carried out at the toe of this well. Bridge plugs were used in the casing to isolate the stages. This study was based on the design of Stage 2, which has a true vertical depth of 8410 ft (2563 m) as shown in Figure 1. The Stage 2 fracturing treatment was pumped with slickwater down the casing, with a pumping rate of 5 bpm (0.013 m^3/s) in the early time. The fractured section was cased and used a single 20-foot long perforation cluster with six shots per foot at 60° phasing. The minimum principal stress is in the horizontal direction, which promotes hydraulic fracture growth vertically.

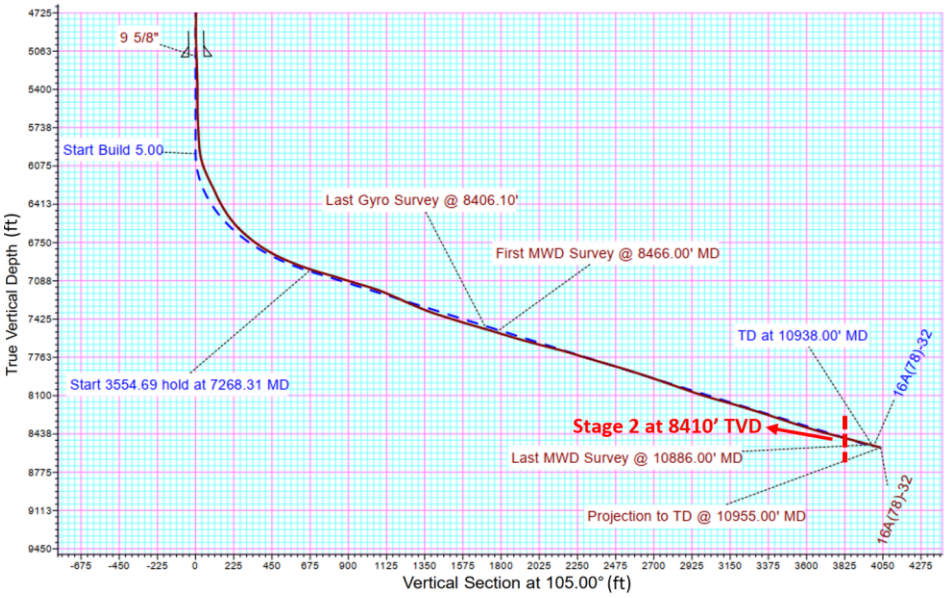

Figure 1: Trajectory of well 16A(78)-32 in a vertical cross-section at the Utah FORGE site and the location of Stage 2 at TVD of 8410 ft.

3. NUMERICAL APPROACH

The simulations of fluid injections and hydraulic fracturing of the rock mass were performed utilizing the numerical code *XSite*, which is a DEM code that implements the synthetic rock mass (SRM) method using a lattice numerical approach. Detailed verifications of hydraulic fracture propagation in different regimes have been carried out, as presented by Damjanac & Cundall (2016) for the viscosity-dominated regime and by Fu et al. (2019) for the toughness-dominated regime. The code has also been compared with analytical criteria developed for 3D interactions between hydraulic fractures and natural fractures, and good agreements were obtained (Fu et al. 2016, 2019).

XSite has several capabilities that make it well-suited for modeling hydraulic fracture initiation and propagation, including the simulation of:

- hydraulic fracture propagation in different regimes;
- general fracture trajectory as a part of the model solution without predefined paths;
- general interaction between multiple hydraulic fractures;
- general interaction between hydraulic fractures and natural fractures/DFN;
- propagation of individual and multiple hydraulic fractures from a stage/different stages; and
- wellbore hydraulics that resolves the distribution of flow rates between the multiple injection points coupled with fracture propagation.

4. NUMERICAL MODEL SETUP

The dimensions of the model are 4 m × 4 m × 2 m (L × W × H). A 1-m long section of the wellbore is placed vertically in local coordinates in the center of the simulation domain. The well casing, cement sheath, and perforation tunnels are explicitly represented, as shown in Figure 2. Note that although the wellbore in Figure 2 appears vertical, in-situ stress conditions were implemented such that the orientation of the wellbore relative to the principal stresses is the same as in the field. Limited by the model size, 12 perforations phased at 60° were simulated, with 6 shots per foot density. It is worth noting that Stage 2 at the Utah FORGE site has a 20-foot perforation interval with 120 perforations, which far exceeds the length of a single perforation cluster for typical hydraulic fracturing wellbores. The main intention of the long-cluster design was to ensure that the perforations intersect with the natural fractures identified through the analysis of wellbore image logs (McLennan et al. 2023). In the numerical model, constrained by the model size, a limited number of perforations were simulated while still allowing the pre-existing fractures to intersect the perforated section as desired. The pumping rate in the simulation is 5 bpm (0.013 m^3/s). The far-field boundaries of the model are fixed, and the directions and magnitudes of the in-situ stresses are chosen to be the same as the in-situ stresses for Stage 2. The model was first brought to equilibrium after excavation and perforation of the wellbore and installation of the casing and cement sheath. Afterwards, fluid was injected into the wellbore and hydraulic fractures were allowed to initiate and propagate. The simulations were stopped before the hydraulic fractures reached the model boundaries.

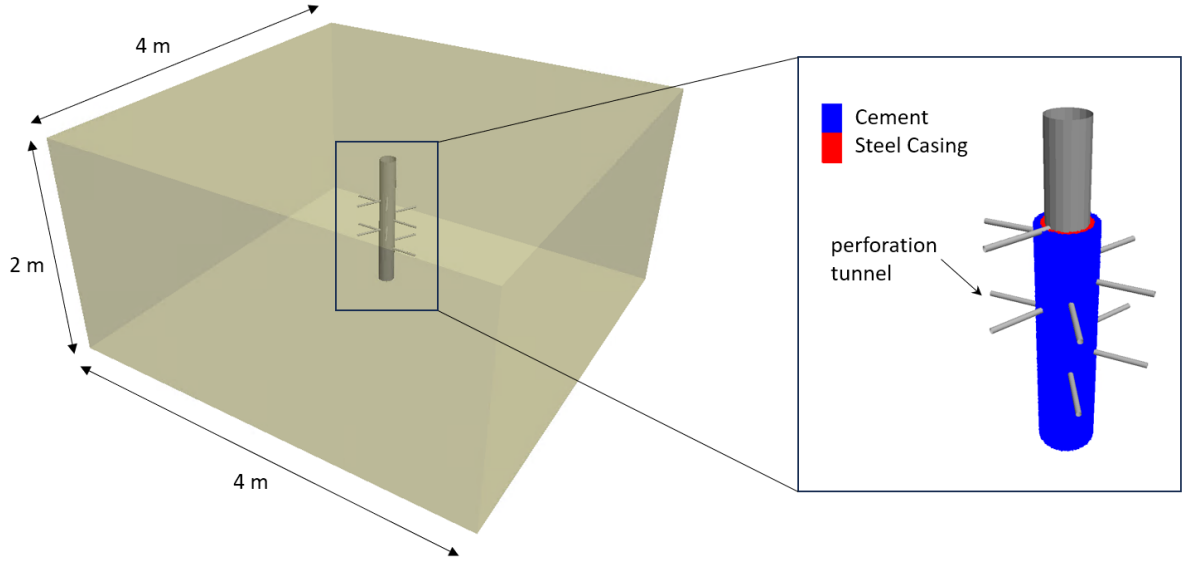

Figure 2: Perforated wellbore in the simulation domain (left) with a detailed plot displaying the perforation tunnels, steel casing, and cement sheath (right).

The rock mass properties, fluid properties, and magnitudes of in-situ stresses are summarized in Table 1. The pre-existing fractures were explicitly represented in the model, as demonstrated in Figure 3, with three highlighted fractures (Fracture ID 86, 181, and 182) intersecting the wellbore at different orientations. Discrete stochastic fractures provided in the DFN have radii in the 0.6 m to 10 m range and orientations are determined based on FMI logs (Finnila et al., 2021). The in-situ DFN is assumed frictional and impermeable until fractures fail in response to stress changes during hydraulic fracture propagation. As shown in Table 2, DFN cohesion and tensile strength are assumed to be zero.

Three simulation scenarios were considered, including:

- Case 1 with a medium cement fracture toughness of 0.5 MPa×m$^{1/2}$, without DFN.
- Case 2 with a high cement fracture toughness of 1 MPa×m$^{1/2}$, without DFN.
- Case 3 with a medium cement fracture toughness of 0.5 MPa×m$^{1/2}$, with DFN.

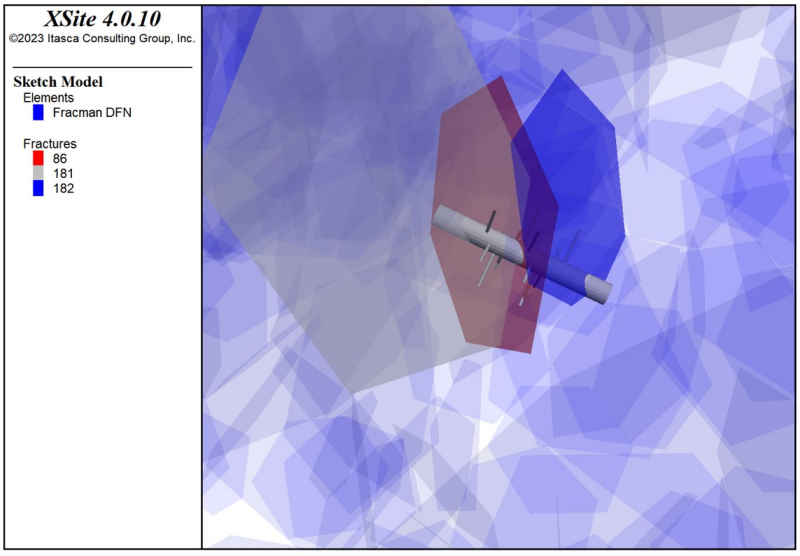

Figure 3: Simulation scenario with DFN filling the domain. The DFN is illustrated in light blue in the background, and three representative natural fractures intersecting the wellbore section are highlighted in red, grey, and dark blue. The plot is oriented such that the simulated wellbore aligns consistently with the actual direction of the wellbore in situ.

Table 1 Input parameters for the near-wellbore model, well 16A(78)-32, stage 2 at TVD of 8410 ft (2563.4 m).

Parameters	Granite	Cement	Casing
Young's modulus, GPa	55	20.7	200
Poisson's ratio	0.26	0.18	0.3
Fracture toughness, MPa×m$^{1/2}$	3	0.5, 1	50
Fluid viscosity, cp	2		
Pore pressure, MPa	23.84		
Minimum horizontal stress, MPa	42.30		
Maximum horizontal stress, MPa	48.45		
Vertical stress, MPa	62.29		

Table 2 Initial DFN properties used in the near-wellbore model.

Parameters	Value
DFN friction angle	37°
DFN cohesion	0
DFN tensile strength	0

5. SIMULATION RESULTS

Simulations were performed to study the role of cement strength in hydraulic fracture growth in the near-wellbore region. Figure 4 shows the net pressure history for two cases with medium and high cement strength (cement fracture toughness = 0.5 MPa×m$^{1/2}$ and 1 MPa×m$^{1/2}$, respectively). Figures 5 and 6 illustrate the modeling results of the two simulation scenarios at representative times, with the wellbore oriented to align with the actual direction of the wellbore in situ in Figure 5, and reoriented close to vertical in the local coordinates to reveal the 3D features of created hydraulic fractures near the wellbore in Figure 6. The model was brought to equilibrium after wellbore perforation and casing/cement installation. Starting from the simulation time of 1.4 s, the net pressure increased rapidly as the hydraulic fluid was injected into the wellbore, until it reached a breakdown pressure of ~ 15.5 MPa for both cases, indicating that the cementation strength has a limited impact on the fracture initiation. The net pressure dropped to ~11 MPa after the breakdown, and then the pressure started to climb gradually for the case with medium cement strength while declining for the case with high cement strength. The increase in propagation pressure indicates the formation of complex fracture geometries that led to tortuous fluid paths. In such situations, the twisting and turning of fluid paths would cause increased resistance to fluid flow, thus causing higher propagation pressure. It's also worth noting from the pressure curves that both cases showed a relatively large pressure drop during fracture propagation, in addition to the early pressure drop at the breakdown point. The case with medium cement strength had a pressure drop of ~ 1.5 MPa at a simulation time of ~1.95 s, while the case with high cement strength developed a larger pressure drop of ~3.5 MPa at a later simulation time of 2.05 s, both indicating the initiation and growth of major hydraulic fracture pathway(s), which became dominated in the near-wellbore fracture propagation.

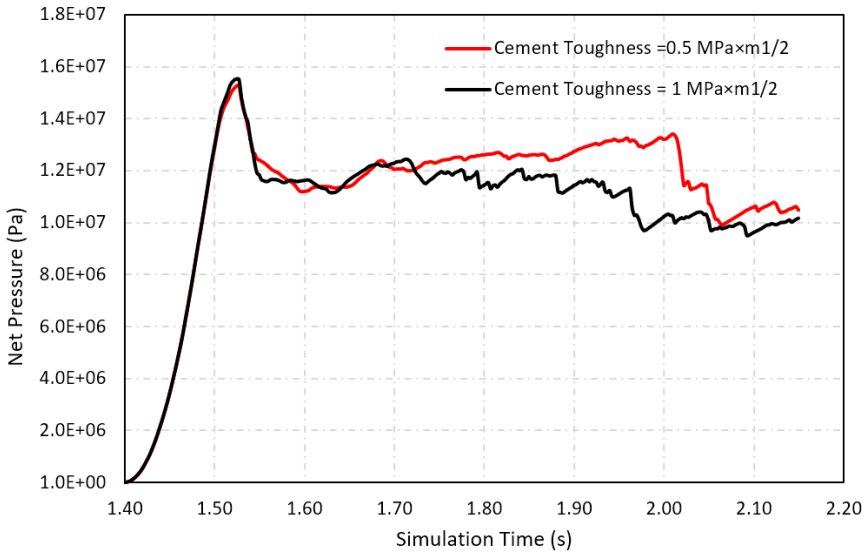

Figure 4: Net pressure history for two simulation scenarios with different cement fracture toughness.

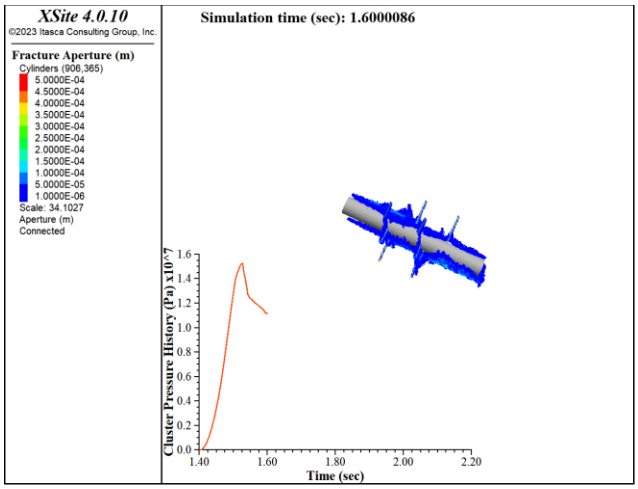

a) t = 1.6 s, Cement toughness = 0.5 MPa×m$^{1/2}$

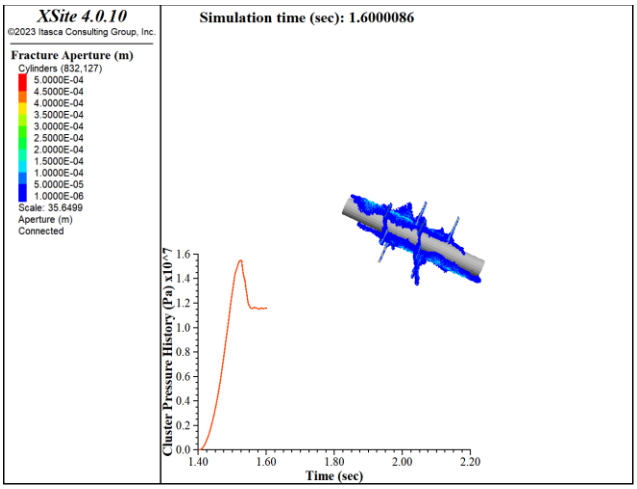

b) t = 1.6 s, Cement toughness = 0.5 MPa×m$^{1/2}$

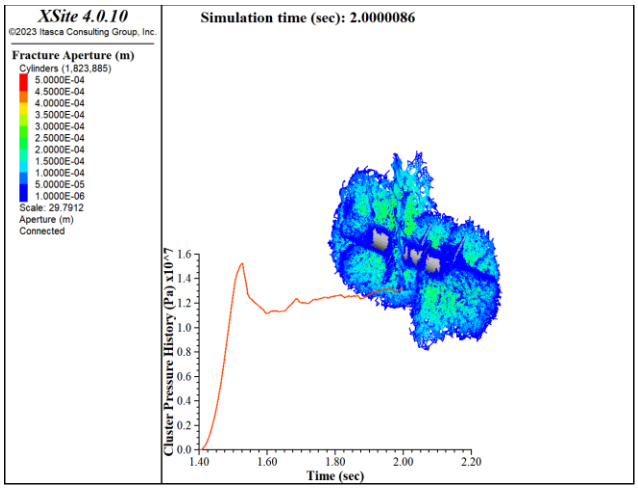

c) = 2.0 s, Cement toughness = 0.5 MPa×m$^{1/2}$

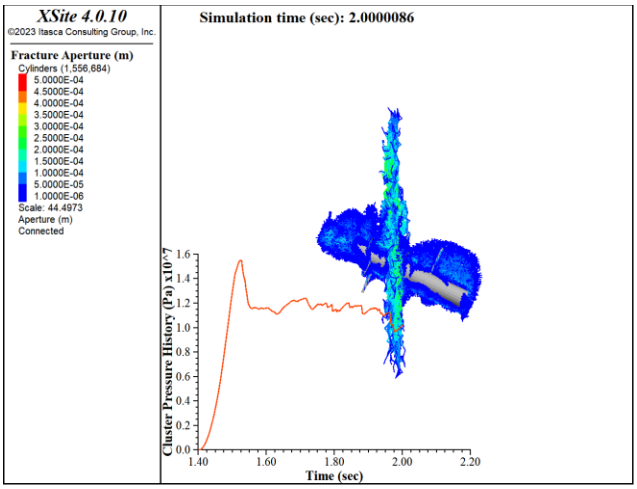

d) t = 2.0 s, Cement toughness = 1.0 MPa×m$^{1/2}$

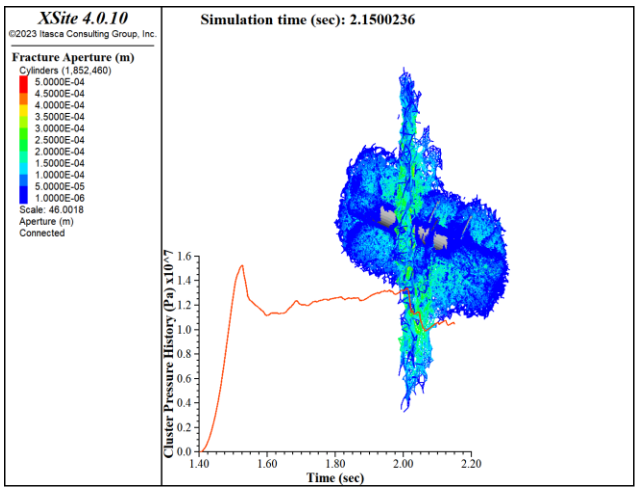

e) = 2.15 s, Cement toughness = 0.5 MPa×m$^{1/2}$

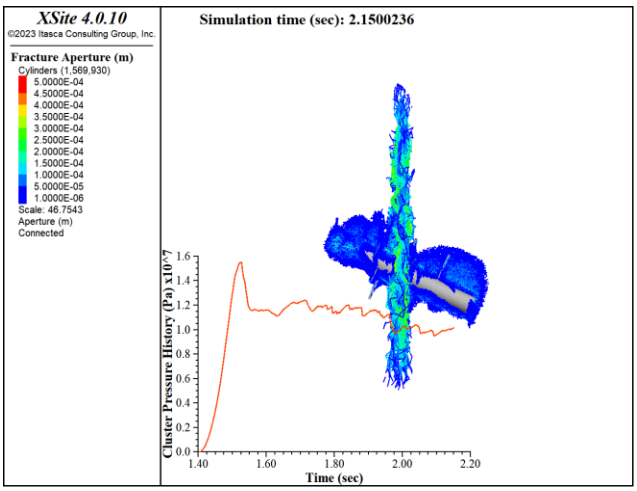

f) t = 2.15 s, Cement toughness = 1.0 MPa×m$^{1/2}$

Figure 5: Modeling results for two simulation scenarios with different cement fracture toughness of 0.5 MPa×m$^{1/2}$ and 1 MPa×m$^{1/2}$ at different times, and the corresponding net pressure history. The simulations were stopped before the fractures reach the model boundary. The plot is oriented such that the simulated wellbore aligns consistently with the actual direction of the wellbore in situ, with the minimum principal stress in the horizontal direction.

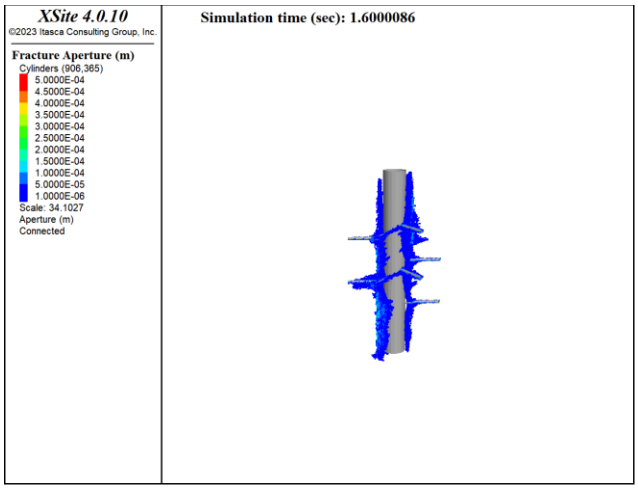

a) t = 1.6 s, Cement toughness = 0.5 MPa×m$^{1/2}$

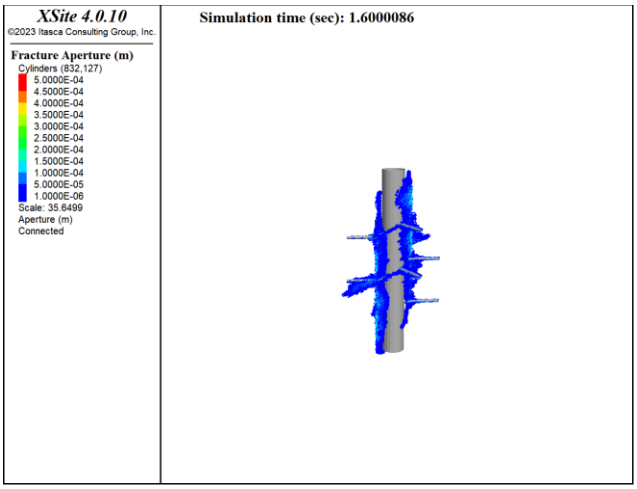

b) t = 1.6 s, Cement toughness = 1.0 MPa×m$^{1/2}$

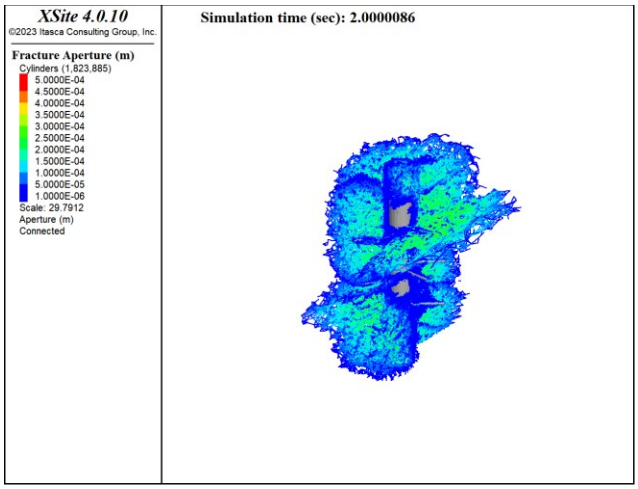

c) = 2.0 s, Cement toughness = 0.5 MPa×m$^{1/2}$

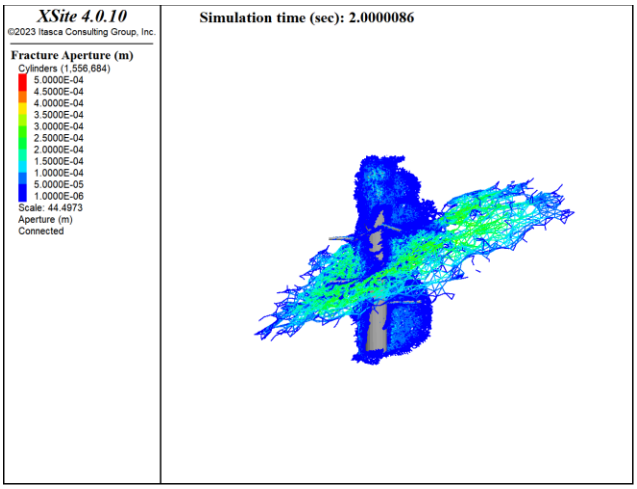

d) t = 2.0 s, Cement toughness = 1.0 MPa×m$^{1/2}$

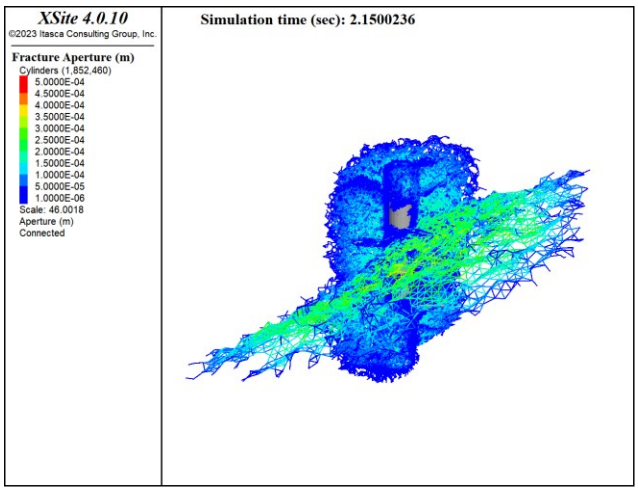

e) = 2.15 s, Cement toughness = 0.5 MPa×m$^{1/2}$

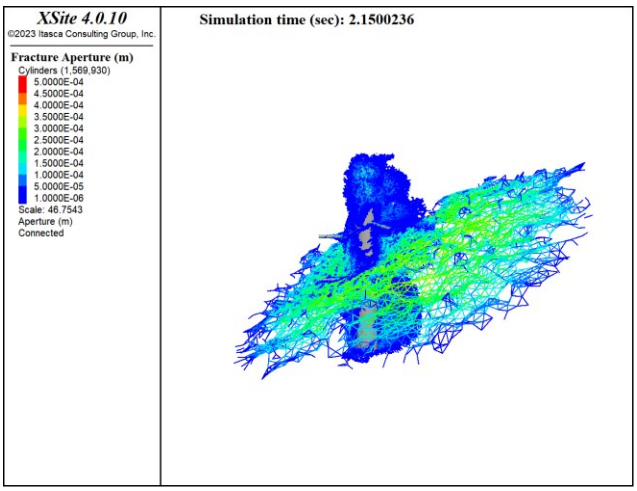

f) t = 2.15 s, Cement toughness = 1.0 MPa×m$^{1/2}$

Figure 6: Modeling results for two simulation scenarios with different cement toughness of 0.5 MPa×m$^{1/2}$ and 1 MPa×m$^{1/2}$ at different times, and the corresponding net pressure history. The simulations were stopped before the fractures reach the model boundary. The view is set such that the wellbore appears close to vertical in the local coordinates to reveal the 3D features of created hydraulic fractures near the wellbore.

The behaviors of hydraulic fracture initiation and propagation in the near-wellbore region can be further illustrated in Figures 5 and 6, which summarize the modeling results for two simulation scenarios with different cement toughness of 0.5 MPa×$m^{1/2}$ and 1 MPa×$m^{1/2}$ at representative times, together with the corresponding net pressure history plot. At early time (t = 1.6 s), both cases showed accumulated cracks along the perforation tunnels and in the cement region along the wellbore (Figures 5a, 5b, 6a, 6b). Considering the similar breakdown pressure obtained from the pressure history plots of the two cases, it can be further inferred that the initiation happened in the granite instead of the cement sheath, because the latter scenario would lead to different breakdown pressures due to the differences in cement strengths otherwise. At a slightly later time (t = 2.0), distinct behaviors were observed in two cases (Figures 5c, 5d, 6c, 6d). Significant fracture tortuosity was formed along the wellbore in the case with medium cement strength, characterized by fracture twisting, rotation, and bifurcation into different directions instead of in the plane of minimum in-situ stress, which is consistent with the observed fluid pressure build-up in the pressure history plot. The case with high cement strength had limited fracture complexity with one major fracture developed vertically to dominate the fracture growth, which also matches the change in the pressure history plot when a sudden pressure drop happened at ~ t = 1.95 s. The simulations were stopped at t = 2.15 s before the fractures reached the model boundaries. It can be observed that, with longer propagation time, both cases developed dominating fractures in the plane of minimum in-situ stress, although the tortuous fracture geometries near the wellbore, once created, could still influence the subsequent fluid circulation and geothermal energy production.

Simulations were also conducted to study the impact of the DFN on hydraulic fracture growth in the near-wellbore region. Figure 7 shows the net pressure history for two cases with and without the DFN, respectively. Similarly, the model was brought to equilibrium after wellbore perforation and casing/cement sheath installation. With fluid injection, the net pressure increased rapidly until it reached the breakdown pressure. The breakdown pressure for the DFN case turned out to be noticeably lower than the case without the DFN. When comparing Figures 8a and 8b at simulation time = 1.6 s, it is found that the hydraulic fractures in the case with the DFN were able to initiate and grow into a pre-existing natural fracture (Fracture ID = 86), thus leading to a breakdown pressure that is ~20% lower than the case without the DFN.

As the fractures continued to grow, the pressure in the case without the DFN showed a gradual increase of ~ 2.5 MPa due to near-wellbore tortuosity, while the pressure in the DFN case increased more rapidly by ~ 6 MPa. Comparing Figures 8b and 8d at simulation time = 1.6 s and 2 s, it can be inferred that as the fractures initiated along the natural fracture, a rapid fluid pressure dissipation happened due to the change of fracture conductivity from impermeable to permeable after the natural fracture failed. Afterwards, the fluid pressure built up quickly due to continuous fluid injection, leading to the rapid pressure increase. In addition, much less near-wellbore tortuosity was induced in the DFN case owing to the pathway formed by pre-existing fractures intersecting the wellbore.

With a longer propagation time, the net pressure in the case without the DFN eventually dropped due to the formation of major dominating fracture(s) and became even lower than the propagation pressure in the DFN case. Such a difference in propagation pressure can be attributed to the impact of the DFN. As shown in Figures 3 and 8, the pre-existing fractures intersected the wellbore at different orientations. In the simulated scenario, Fracture 86 emerged as the most favorable pathway for the initiation and growth of hydraulic fractures. This preference is attributed to the fracture's orientation close to the plane of the minimum in-situ stress. However, since it still formed a noticeable angle from the plane of the minimum in-situ stress, a higher propagation pressure was thus needed than the case without the DFN, in which the fractures were able to reorient and grow vertically in the direction with the least resistance (i.e., perpendicular to the direction of minimum in-situ stress). Given a longer propagation time, a similar reorientation would also be expected in the DFN case, if not being further disturbed by other pre-existing fractures.

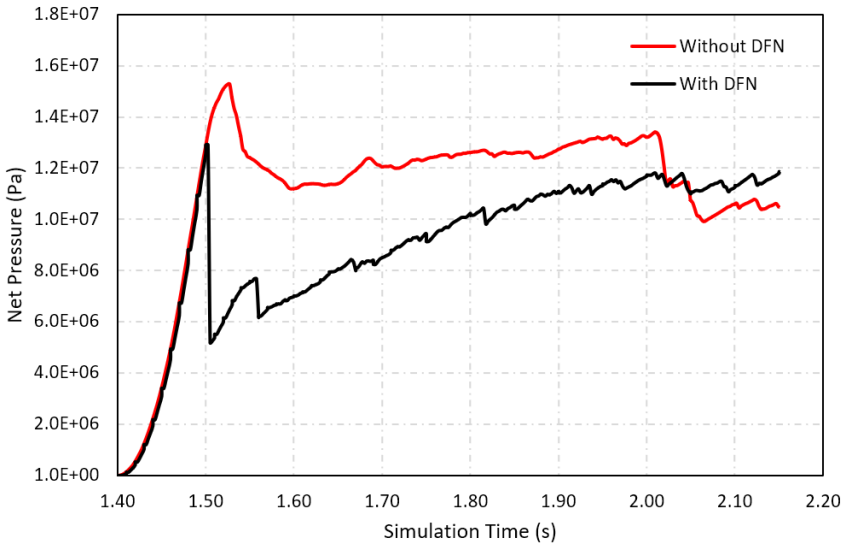

Figure 7: Net pressure history for simulation scenarios with/without DFN.

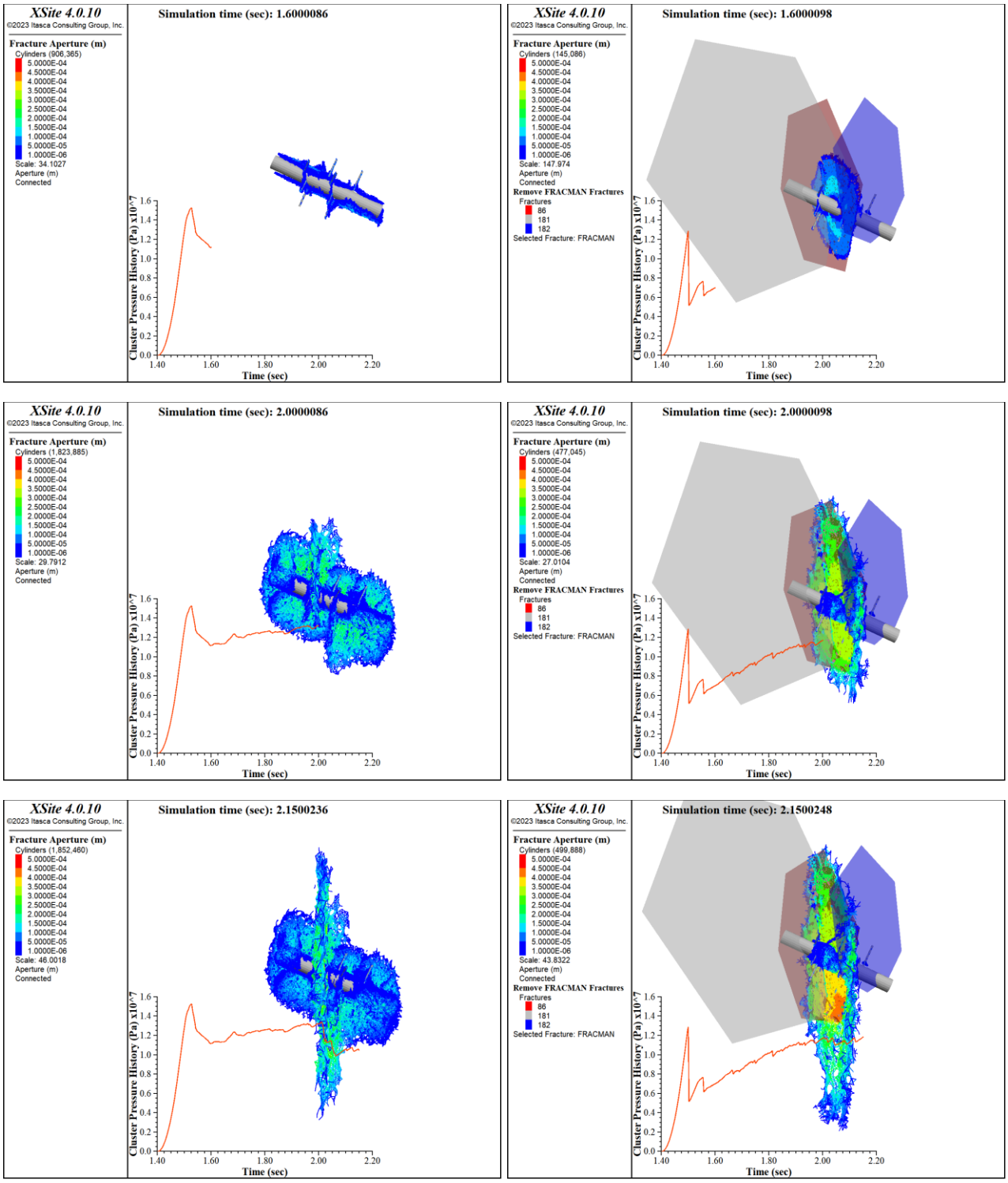

Figure 8: Modeling results for two simulation scenarios with/without DFN at different times, and the corresponding net pressure history. Note that only representative natural fractures (Fractures 86, 181, 182) intersecting the wellbore section are illustrated. The plot is oriented such that the simulated wellbore aligns consistently with the actual direction of the wellbore in situ.

6. CONCLUSIONS

Acquiring a comprehensive understanding of near-wellbore fracture behaviors is crucial for many aspects of EGS, ranging from reservoir stimulation effectiveness to fluid circulation and heat transfer efficiency. In this study, the hydraulic fracture initiation and growth in the near wellbore region was investigated using a fully coupled hydro-mechanical model. Complex fracture initiation, competing, and merging behaviors were captured under the influence of different cementation strengths and the existence of the DFN. Fluid pressure history was discussed in detail to reveal the correlation between fluid pressure characteristics and fracture propagation behaviors near the wellbore.

In summary, the study found that the strength of the cement sheath strongly influences the near-wellbore fracture behaviors. With a relatively lower cement strength, more complex fractures were formed with fracture paths twisting and curving, leading to increased resistance to fluid flow and pressure built up during fracture propagation. Such near-wellbore tortuosity can reduce the communication path between the wellbore and the near reservoir. This is even more critical if proppants are planned in the future designs at the Utah FORGE Site. Cement sheath with higher fracture toughness is recommended to prevent potential proppant bridging and premature screenouts.

The simulation results also showed that the existence of the DFN intersecting the wellbore section at a favorable angle (i.e., close to the plane of the minimum in-situ stress) can effectively reduce the breakdown pressure. This is consistent with the design concept for Stages 2 and 3 at Utah FORGE Site, which was to ensure that perforations intersected with the natural fractures. In the simulated case with the DFN, a decrease of ~ 20% in peak net pressure was observed, which helped facilitate breakdown in the high-strength reservoir, as well as much less severity of near-wellbore tortuosity owing to the pathway formed by pre-existing fractures.

ACKNOWLEDGEMENTS

Funding for this work was provided by the U.S. Department of Energy under grant DE-EE0007080 "Enhanced Geothermal System Concept Testing and Development at the Milford City, Utah FORGE Site." We thank the many stakeholders supporting this project, including Smithfield, Utah School and Institutional Trust Lands Administration, and Beaver County, as well as the Utah Governor's Office of Energy Development.

This research made use of the resources of the High Performance Computing Center at Idaho National Laboratory, which is supported by the Office of Nuclear Energy of the U.S. Department of Energy and the Nuclear Science User Facilities under Contract No. DE-AC07-05ID14517.

REFERENCES

Damjanac, B., & Cundall, P. (2016). Application of Distinct Element Methods to Simulation of Hydraulic Fracturing in Naturally Fractured Reservoirs. Computers and Geotechnics, 71, 283–294. https://doi.org/10.1016/j.compgeo.2015.06.007

Damjanac, B., Detournay, C., & Cundall, P. (2020). Numerical Simulation of Hydraulically Driven Fractures. Modelling Rock Fracturing Processes: Theories, Methods, and Applications, 531–561.

Finnila, A., Doe, T., Podgorney, R., Damjanac, B., & Xing, P. (2021). Revisions to the Discrete Fracture Network Model at Utah FORGE Site, GRC Transactions, Vol. 45.

Fu, W, Ames, B. C., Bunger, A. P., & Savitski, A. A. (2016). Impact of Partially Cemented and Non-persistent Natural Fractures on Hydraulic Fracture Propagation. Rock Mechanics and Rock Engineering, 49(11), 4519–4526. https://doi.org/10.1007/s00603-016-1103-0

Fu, W, Savitski, A. A., Damjanac, B., & Bunger, A. P. (2019). Three-Dimensional Lattice Simulation of Hydraulic Fracture Interaction with Natural Fractures. Computers and Geotechnics, 107, 214–234. https://doi.org/10.1016/j.compgeo.2018.11.023

McLennan, J., England, K., Rose, P., Moore, J. & Barker, B. (2023). Stimulation of a High-Temperature Granitic Reservoir at the Utah FORGE Site. In SPE Hydraulic Fracturing Technology Conference and Exhibition. OnePetro.

Itasca. (2023). XSite — Hydraulic Fracture Simulation of 3D Fracture Networks (4.0).